

STUDY OF CORROSION BEHAVIOR OF OIL GATHERING FACILITIES WITH CO₂ FLOODING IN LOW-PERMEABILITY OILFIELDS

Zhihua Wang,¹ Lei Zhang,¹ Tianyu Yu,^{1,2} and Mengmeng Xu¹

Carbon dioxide (CO₂) gas flooding for enhancement of oil recovery is known to face challenges such as corrosion and scaling of oil-gathering facilities and environmental pollution. The corrosion behavior of the gathering facilities must be studied to select the optimum measures for protecting them from the corrosive effect of CO₂. Surface corrosion of the separator, a key problem with using CO₂, is evaluated in the present work. The corrosion characteristics, corrosion rate, and corrosion products in different functional areas of the facility were determined by the weight-loss method, scanning electron microscopy (SEM), and x-ray diffraction (XRD) analysis. The results indicate that pitting corrosion is the main characteristic of Fe-360 A steel facilities and that the average corrosion rate in vulnerable areas can reach 0.1358 mm/yr with formation of Fe₂O₃ and FeS. The combined effects of contact time and CO₂ volume in conjunction with the activity of sulfate-reducing bacteria influence the corrosion kinetics and mechanism of Fe-360 A steel. The results are of great significance for minimizing corrosion using chemical inhibition and proper selection of materials that come into contact with CO₂.

Keywords: CO₂ corrosion, gathering facility, corrosion coupon, CO₂ gas flooding, low-permeability oil field.

¹Key Laboratory of Enhanced Oil & Gas Recovery, Northeast Petroleum University, Daqing, China.

²Oil and Gas Engineering, School of Civil, Environmental and Mining Engineering, University of Western Australia, Perth, Australia. E-mail: zhihua_wang@126.com. Translated from *Khimiya i Tekhnologiya Topliv i Masel*, No. 6, pp. 79 – 84, November – December, 2017.

Development of operating methods and enhanced oil recovery (EOR) at low-permeability oil reservoirs are required to address the challenge of declining oil production and a transition to the high water-cut period [1, 2]. Gas flooding has unique advantages due to the gas chemical properties, i.e., small molecules, large intermolecular distances, low density, low viscosity, and low flow resistance with compressibility. It is already widely used for EOR in addition to chemical and steam flooding [3]. It has minimal environmental impacts. CO₂ gas is the second least expensive flooding fluid after H₂O and has been used in EOR for many years. CO₂ injection has been used as a commercial EOR process since the 1970s [4]. Currently, greater than 20,000 tons of CO₂ per day are delivered for EOR. In America, CO₂ flooding enabled crude oil production to be increased with the future efficiency of the method estimated at 4-47 billion barrels of oil [6-8].

Several CO₂ EOR projects have recently emerged in China under the support of the government. Basic laboratory research and pilot tests of a model process were conducted. It was shown that the low viscosity of CO₂ causes it to channel and finger toward the production well and to bypass large amounts of oil during oil recovery with an advancing oil—water front. This effect is especially evident in high heterogeneity reservoirs [9, 10]. CO₂ gas appears in the produced liquid to different degrees and dissolves, changes the solution pH, and causes chemical reactions that promote corrosion.

Corrosion has held back the development and broad application of CO₂ flooding technology. Gathering facilities are most susceptible to corrosion in practice. Consequently, gathering facility areas were selected for the studies. The research results will be helpful for understanding the corrosion mechanism, developing methods for protecting the facility, and promoting the mature application of CO₂ flooding in low-permeability oilfields.

Figure 1 shows a scheme for gathering EOR products from CO₂ flooding (at Daqing oilfield, China).

Oil from a group of production wells is sent through a pipeline to the manifold. The resulting mixture of oil, gas, and water is transported through metering devices and fed into the separator for preliminary phase separation. The oil mixture flows from the separator into the dehydration station for purification. A tracing band is wound around production wellheads to prevent freezing and blockage due to escaping CO₂ and the sharp temperature and pressure changes caused by it. Polyurethane foam is used for insulation of the oil-mixture gathering and separating pipelines. The phase separator in which heating, buffering, gas separation, and free water sedimentation occur is the main gathering facility. Considering the relatively high construction costs and operating pressures from 30 to 45 psi, carbon steel Fe-360 A is usually used to fabricate the gathering facility.

Wells with CO₂ flooding were chosen for the study. Samples of the oil—water mixture and gas were taken at the wellhead. The gas composition was analyzed by GC (7890A chromatograph, Agilent Technologies); the liquid composition, by ion chromatography (ICS-1100, Dionex). The number of bacteria was determined using serial dilutions in broth. Corrosion was determined using coupons (50 × 25 × 2 mm) of

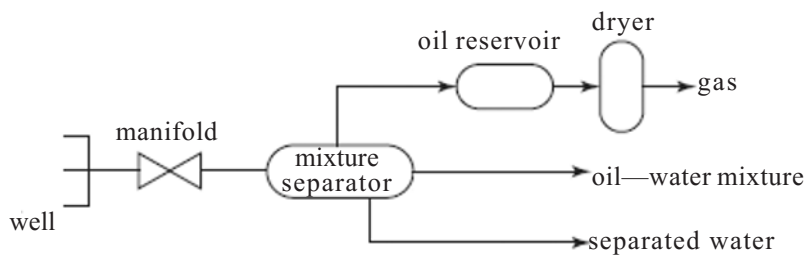


Fig. 1. Scheme for gathering oil-recovery products from CO₂ flooding.

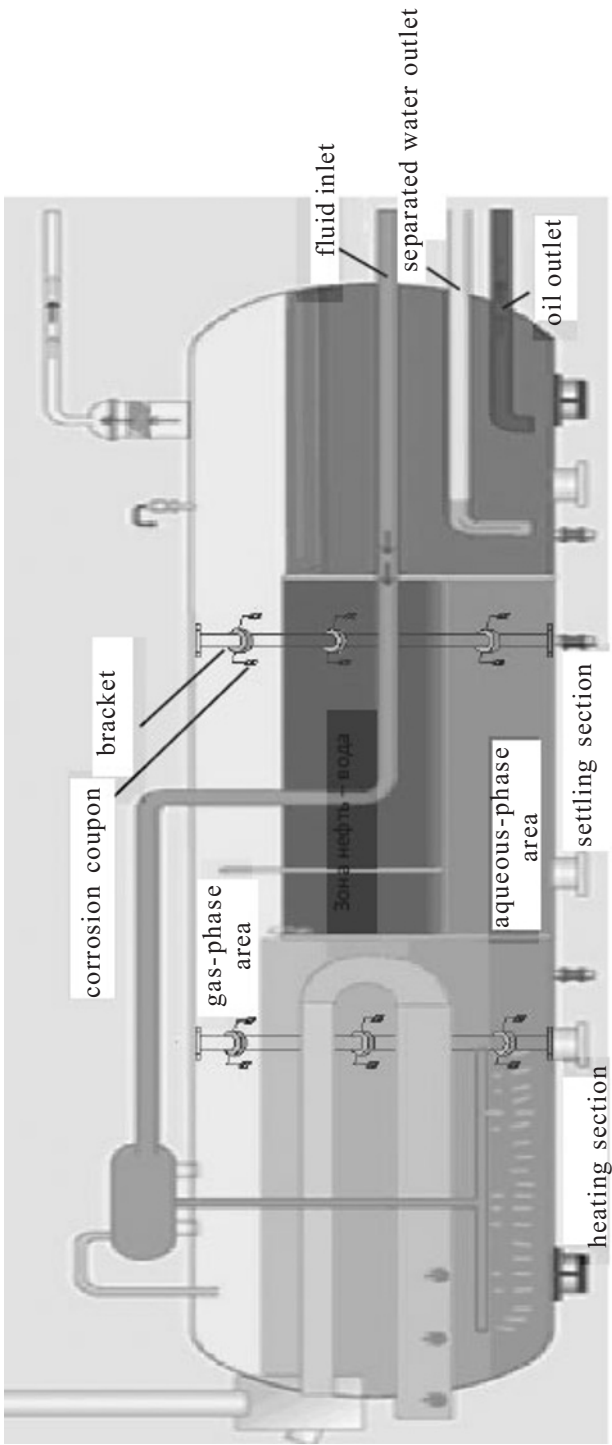


Fig. 2. Experimental setup for evaluating corrosion behavior.

carbon steel Fe-360 A, i.e., the same material as the gathering facilities. The gas-phase, oil—water-mixture, and aqueous-phase areas in the separator were determined. Corrosion coupons were suspended on the bracket in each area perpendicular to the flow direction. Two brackets with samples were placed in the heating and settling sections, respectively (Fig. 2). Coupons were prepared by soaking in Me₂CO for 20 min followed by ultrasonic cleaning, soaking in anhydrous alcohol for 5 min, drying, weighing, and numbering.

After eight months, the brackets were removed. The coupon surfaces were cleaned of greasy deposits using an organic solvent. Then, corrosion products were rinsed off with acid. The coupons were dried and weighed. The corrosion rate was determined from the weight loss. The morphologies of the corrosion coupons were studied on an S-3400N scanning electron microscope (SEM, Hitachi Ltd.). The compositions of the corrosion products were analyzed using energy-dispersive x-ray (EDX) spectroscopy on an EMAX spectroscope (Hitachi Ltd.). X-ray diffraction (XRD) analysis used a TD3500 instrument (Dandong Tongda Science and Technology Co., Ltd.). The following corrosion mechanism was proposed based on the results.

The mixture parameters at the wellhead were temperature, 38°C; average salinity, 4301.48 mg/L; pH, 7.13; and HCO₃⁻ and Cl⁻ concentrations, 1741.16 and 915.7 mg/L, respectively. Sulfate-reducing bacteria (SRB) were also detected. Besides, the average contents of CO₂ and H₂S in the associated gas were 16.75 and 2.16%, respectively, because the wells had gas channels. Therefore, the chemical composition and properties of the mixture undoubtedly created corrosive conditions.

The corrosion rate during the experiment was calculated using the equation

$$CR = \frac{87.6w}{\rho At}$$

where *CR* is the corrosion rate (mm/yr); *w*, weight loss (mg); *ρ*, density (g/mm³); *A*, experimental coupon area (cm²); and *t*, immersion time (h).

Figure 3 shows experimental corrosion rates for different gathering-facility areas. It can be seen that the average corrosion rates in the gathering facility were much higher than the limiting allowable value of 0.076 mm/yr except for the gas-phase area in the heating section and the oil—water-mixture area in the settling section.

Figure 4 shows the morphologies of experimental coupons from different areas. It can be seen that corrosion occurred mainly in the oil—water-mixture area of the heating section and was dominated by pitting

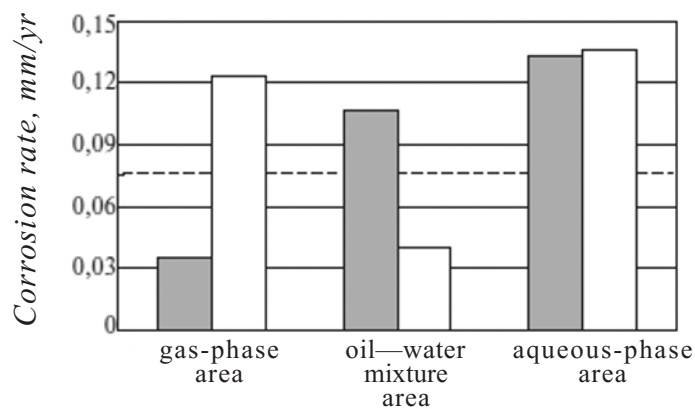


Fig. 3. Coupon corrosion rate in gathering facility: ■ and □, heating and settling sections, respectively; dashed line shows limiting allowable corrosion rate.

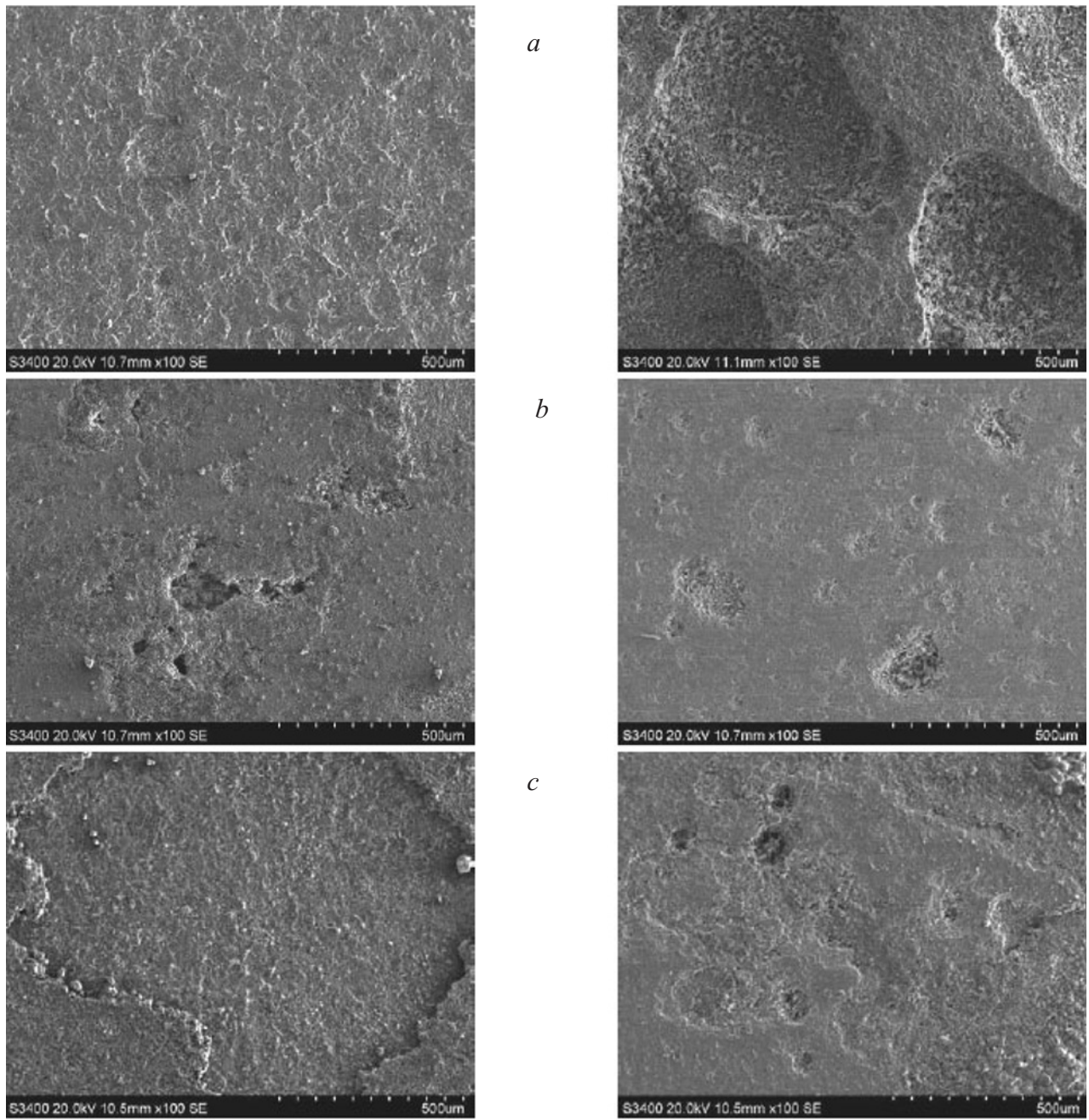


Fig. 4. Surface morphologies of corrosion coupons in heating (left) and settling sections (right) (100 \times magnification): a, b, c) gas-phase, oil—water-mixture, and aqueous-phase areas, respectively.

corrosion. Relatively slight uniform corrosion appeared on the coupon surface in the gas-phase area and was attributed to incomplete phase separation of the oil—gas—water mixture in the heating section and associated gas in the gas phase. Correspondingly, the oil—water mixture contained large amounts of residual water that was not separated into the aqueous phase so that corrosion was facilitated. Corrosion appeared faster in the

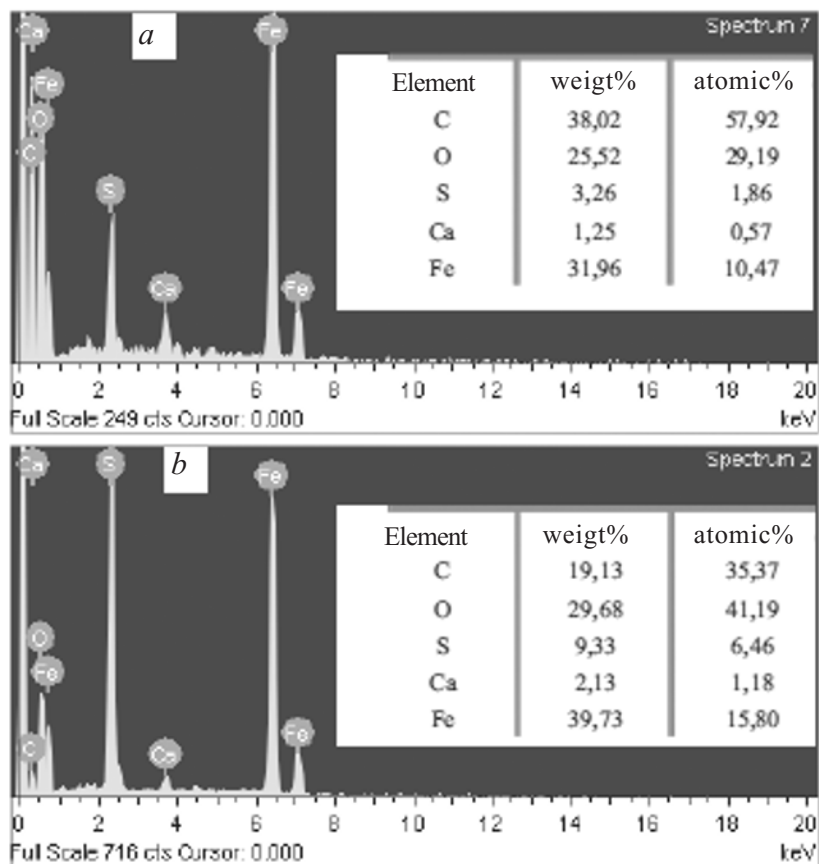


Fig. 5. Energy-dispersive x-ray analysis of corrosion products in aqueous- (a) and gas-phase areas (b) of the heating section.

gas- and aqueous-phase areas in the separator settling section and was also dominated by pitting corrosion. Coupons placed in the oil—water-mixture area had only slight corrosion because the produced liquid was fully separated in the settling section after heating. The CO_2 escaped to the gas-phase area and dominated the corrosion mechanism in the presence of water so that corrosion pits emerged. Coupon surfaces were in contact mainly with the oil phase in the oil—water-mixture area after separation of free water. This naturally restrained corrosion. The corrosion characteristics in the aqueous-phase area were similar to those in the heating section although the corrosion rate in the gas phase increased significantly. Further studies of the morphological characteristics confirmed the quantitative analyses of the corrosion rate.

Analytical results showed that the corrosion products in all gathering facility areas were similar. The elemental composition was analyzed by EDX and detected C, O, Fe, S, and Ca (Fig. 5). The surface morphology revealed powder precipitation surrounded by crystals (Fig. 6). The outer appearance suggested that the corrosion products consisted mainly of Fe_2O_3 with small amounts of FeS. Quantitative XRD analysis showed that the Fe_2O_3 content reached 70% (Fig. 7). The analytical data indicated that the corrosion behavior was determined by the presence of CO_2 .

The CO_2 corrosion mechanism was affected by several factors including the temperature, pH value, flow rate, and CO_2 pressure. It was reported that the corrosion rate and pitting severity increased with decreasing pH and increasing CO_2 pressure [11, 12]. Generally, the main reaction was dissolution of CO_2 in

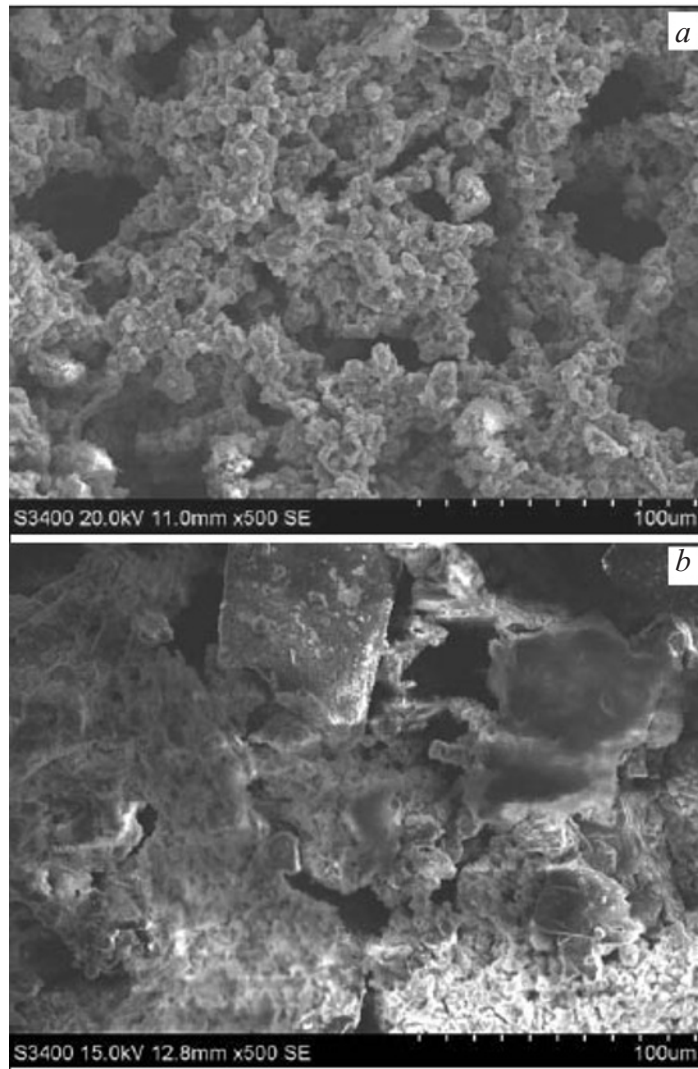
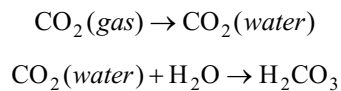


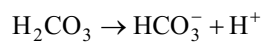
Fig. 6. Surface morphologies of corrosion products in the aqueous- (a) and gas-phase areas (b) of the heating section (500 × magnification).

water to form carbonic acid (H_2CO_3). At the same time, Fe^{2+} diffused into the solution to form FeCO_3 as the corrosion product when the Fe^{2+} and CO_3^{2-} concentrations exceeded the solubility product of FeCO_3 . The chemical reactions were as follows.

CO_2 is sparingly soluble in water and produces H_2CO_3 :



H_2CO_3 dissociates partially in two steps to form bicarbonate (HCO_3^-) and carbonate (CO_3^{2-}) ions:



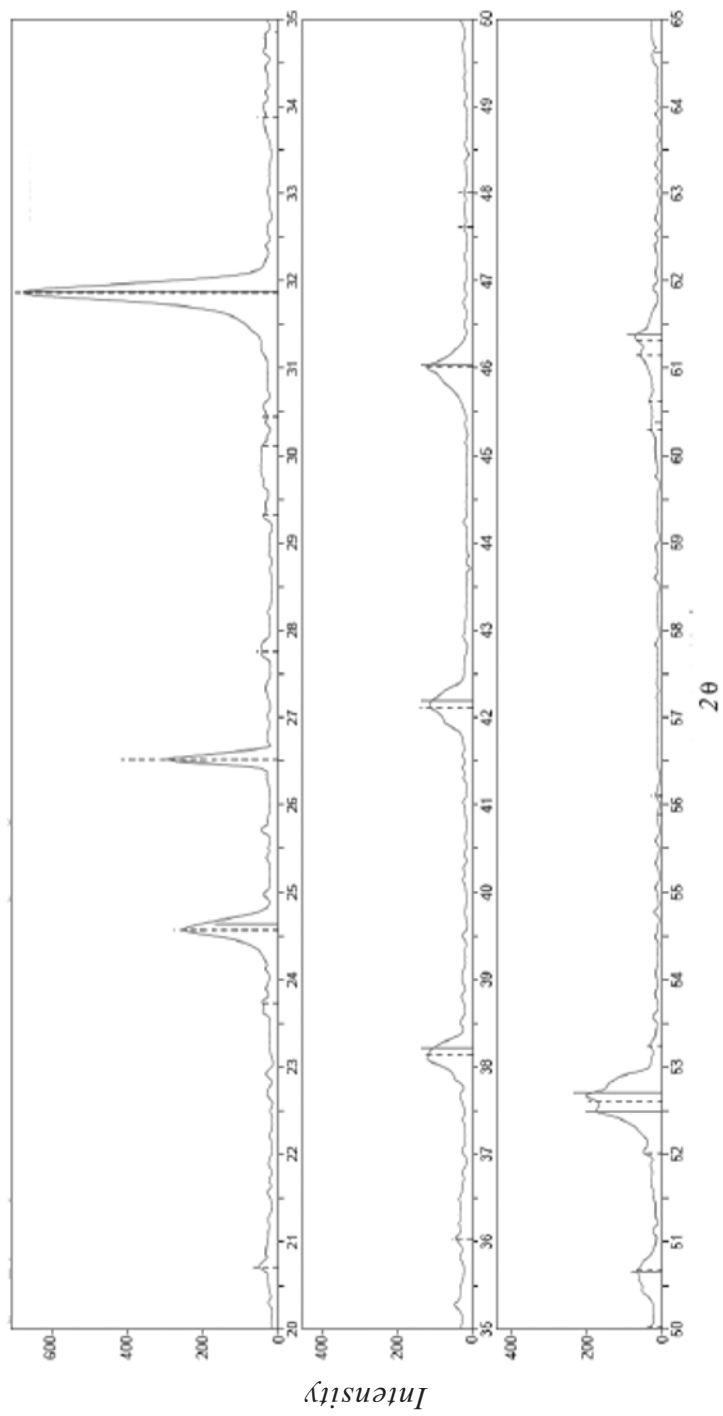
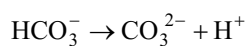
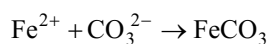


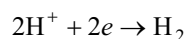
Fig. 7. X-ray diffraction analysis of corrosion products.



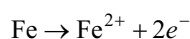
Solid iron carbonate is formed:



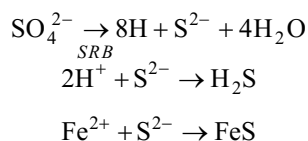
Several electrochemical reactions occur during the CO₂ corrosion process. Adsorption of H₂CO₃ on a steel surface is followed by reduction of H⁺:



Iron oxidation occurs simultaneously:



As a rule, FeCO₃ formation plays an important role in the corrosion behavior because the FeCO₃ layer prevents mass transfer of the corrosive species and protects the steel surface from the corrosive environment. In this sense, the presence of the FeCO₃ layer should enable the CO₂ corrosion rate to be controlled. However, the large number of SRB in the produced liquid also cause additional electrochemical corrosion behaviors and promoted corrosion of the steel surface despite the layer of deposited FeCO₃:



Furthermore, differences in the ion concentrations activated local galvanic corrosion after the formation of corrosion pits of different depths and origins. High concentrations of Cl⁻ in the produced liquid caused destructive pitting corrosion and led to stress cracking corrosion behavior of the facility structures. In addition, CO₂ not only contributed directly to the main electrochemical reaction but also was involved in hydrogen reduction on contact of carbon steel Fe-360 A with H₂S dissolved in water.

Thus, the complex characteristics of the produced liquid with CO₂ were inherent causes of corrosion and scaling in the gathering facility. The selection of facility materials and the limited budget for oilfield development were external causes. The oil—gas—water separator was used as an example to show that the degree of gas channeling, CO₂ escape time, and separation performance of water were responsible for differences in the corrosion behavior.

Pitting corrosion with the formation mainly of Fe₂O₃ and FeS was the main corrosion behavior of steel Fe-360 A in the presence of CO₂. The corrosion kinetics and mechanism depended on combined effects of CO₂ and SRB in the produced mixture.

ACKNOWLEDGMENTS

The work was financially supported by the State Key Program of the National Natural Science Foundation of China (Grant No. 51534004) and the University Nursing Program for Young Scholars with Creative Talents in Heilongjiang Province (Grant No. UNPYSCT-2015074).

REFERENCES

1. D. Q. Niu, J. W. Liang, and S. Z. Wang, *Chem. Technol. Fuels Oils*, 50, No. 6, 494-500 (2015).
2. H. Y. Zhong, Z. H. Wang, and E. M. Cao, *Int. J. Oil, Gas Coal Technol.*, 6, No. 5, 507-516 (2013).
3. O. Arjmand and A. Roostaei, *Res J. Appl. Sci., Eng. Technol.*, 4, No. 17, 3065-3068 (2012).
4. B. T. Hoffman and S. Shoaib, *J. Energy Resour. Technol.*, 136, No. 2, 1-10 (2014).
5. R. B. Alston, G. P. Kokolis, and C. F. James, *SPE J.*, 25, No. 2, 268-274 (1985).
6. S. H. Stevens and J. Gale, *Oil Gas J.*, No. 20, 40 (2000).
7. K. Su, X. W. Liao, and X. L. Zhao, *J. Pet. Sci. Eng.*, 125, 128-135 (2015).
8. F. Gozalpour, S. R. Ren, and B. Tohidi, *Oil Gas Sci. Technol.*, 60, No. 3, 537-546 (2005).
9. B. S. Ju, T. L. Fan, and Z. X. Jiang, *J. Pet. Sci. Eng.*, 109, 144-154 (2013).
10. Y. Liu, J. X. Li, Z. H. Wang, et al., *Environ. Earth Sci.*, 73, No. 10, 5891-5904 (2015).
11. A. H. Mustafa, B. Ari-Wahjoedi, and M. C. Ismail, *J. Mater. Eng. Perform.*, 22, No. 6, 1748-1755 (2013).
12. G. X. Zhao, X. H. Lu, J. M. Xiang, et al., *J. Iron Steel Res. Int.*, 16, No. 4, 89-94 (2009).